PCCP

PAPER

View Article Online
View Journal | View Issue

Cite this: *Phys. Chem. Chem. Phys.*, 2015, **17**, 10737

Functionalization of a GaSe monolayer by vacancy and chemical element doping

L. Ao,[a] H. Y. Xiao,*[a] X. Xiang,[a] S. Li,[b] K. Z. Liu,[c] H. Huang[c] and X. T. Zu*[ad]

Received 22nd January 2015,
Accepted 13th March 2015

DOI: 10.1039/c5cp00397k

www.rsc.org/pccp

Based on first-principles plane-wave calculations, functionalization of the two-dimensional single-layered GaSe structure through vacancy and chemical element doping has been investigated. Our calculations show that the pristine GaSe monolayer, which is normally a non-magnetic, indirect-band-gap semiconductor, can induce net magnetic moments by introduction of Ga mono-vacancy, Ga di-vacancy, and $GaSe_3$ and Ga_2Se_6 vacancy complexes. Magnetic moments can also be induced by selectively doping specific transition-metal atoms as well as A group atoms. The introduced donor or acceptor states are localized in the band gap, which expands the utilization of the single-layered GaSe in nanoelectronics and spintronics. In spite of the intrinsic p-type character of the two-dimensional GaSe material, substitution of Si for Ga and substitution of Cl for Se exhibit n-type character at relatively low dopant concentrations. These findings will provide useful supplements to the experimental studies on the newly synthesized two-dimensional layered metal monochalcogenides, which allows us to go beyond the current scope that is limited to applications within graphene, BN, and transition-metal dichalcogenide-based nanostructures.

1. Introduction

Two-dimensional (2D) materials have attracted great attention due to their remarkable physical properties and prospects for technological applications in a variety of fields. As the first prototype, the fascinating material graphene has been extensively studied for its unusual electrical, optical, magnetic, and mechanical properties.[1–10] However, the absence of a band gap limits its application as a transistor. One of the alternative way is to search for other novel 2D materials that are analogous to graphene but with semiconducting characteristics and other promising properties.

Two dimensional GaSe is a new kind of layered metal monochalcogenide materials and has been successfully synthesized by various kinds of methods in recent years.[11–13] The GaSe monolayer is Se–Ga–Ga–Se tetra-layered with a Ga–Ga dimer covalently bonded to six Se atoms, with D_{3h} symmetry and a lattice constant of 3.74 Å.[14] The emerging 2D GaSe opens a fascinating new chapter in nano-electronic applications. Its intriguing properties, such as high orders of on–off ratios and photo-responsivity, mechanically robust nature and thermal stability, demonstrate its potential for photo-detector, sensor, and field-effect transistor (FET) applications.[12] The quantum confinement effects,[15] strain response,[15] topological properties,[16] p-type doping behavior[17] and solar water-splitting application[18] of the GaSe monolayer. However, as an emerging family of 2D materials, information about the fundamental properties of the GaSe nanomaterial is still limited in the literature. For example, GaSe has many polytypes (β, ε, γ, *etc.*), while few studies have been carried out on their optical properties. Thus far, the refractive index and dielectric constant for bulk and thin film ε-GaSe have been reported by Zhang *et al.*[19] and Ma *et al.*,[15] but the optical data for other phases are scarce. To gain fundamental insights into the application of GaSe as transistors, nanoelectronics and nanospintronics, functionalizing GaSe material is thus highly desirable to modify and manipulate its electronic and magnetic properties.

A large number of experimental and theoretical studies indicate that introduction of vacancies can influence the electronic and magnetic properties of low-dimensional materials significantly, which provides an effective approach to functionalize the host materials.[20–28] Vacancy defects in the nanostructure can be controllably achieved by chemical vapor deposition (CVD), field evaporation, and electron irradiation method, *etc.*[22,25,29,30] Previous studies indicated that C-vacancy decorated graphene can be magnetized, with a magnetic moment increase of 1.12–1.53 μ_B, as the defect concentration decreases from 20% to 0.5%.[31] In the h-BN monolayer, a single B vacancy acts as a p-type defect and can induce a magnetic moment of 3 μ_B, while a

[a] *School of Physical Electronics, University of Electronic Science and Technology of China, Chengdu 610054, China. E-mail: hyxiao@uestc.edu.cn; Fax: +86-28-83202130; Tel: +86-28-83202130*
[b] *School of Material Science and Engineering, University of New South Wales, Sydney 2052, Australia*
[c] *Science and Technology on Surface Physics and Chemistry Laboratory, Mianyang 621900, China*
[d] *Institute of Fundamental and Frontier Sciences, University of Electronic Science and Technology of China, Chengdu 610054, China. E-mail: xtzu@uestc.edu.cn*

single N vacancy plays a role of an n-type defect, producing a magnetic moment of 1 μ_B.[32] For MoS_2, it has been found that the ground state of the 2D crystal with a MoS_6 vacancy cluster is spin-polarized with a large magnetic moment of 6 μ_B.[21] Besides, vacancies can play a major role in thermal transport as well as mechanical behavior of nanomaterials,[33] or make them promising for the application in sensors.[34,35] For example, the diffusion and reactivity of oxygen vacancies in ceria nanoparticles results in high oxygen storage capability.[34] Investigation of the effects of vacancy on the electronic and magnetic properties of 2D GaSe is thus of great interest for functionalization of the nanomaterials. However, to date, a systematic study of the vacancy effects on the electronic and magnetic properties of the GaSe monolayer has not been reported yet.

Another promising route to tune the carrier density and manipulate the electronic and magnetic properties is engineering substitutions in nanostructures. For example, recent experimental and theoretical studies indicated that n-type character of MoS_2 can be achieved by Re doping,[36] while Nb or Au doping results in p-type character.[37,38] Çakır *et al.* proposed that Mo and P are the most promising candidates for p-type doping of 2D ReS_2, while Cl is an ideal candidate for n-type doping.[39] Besides, several experimental and theoretical studies have reported that magnetism in non-magnetic nanomaterials can be induced and manipulated by substitution of transitional metal (TM) atoms.[39–44] For example, embedding V, Cr, Mn, Co, Cu and Zn atoms yielded several magnetic moments in vacancy decorated graphene.[44] Investigation of long-range ferromagnetic ordering in Mn-doped MoS_2, $MoSe_2$, $MoTe_2$ and WS_2 has been reported for Mn concentration less than 5%.[42] Meanwhile, TM-doped 2D materials, such as Fe, Co, Ni, or Cu-doped MoS_2, exhibit half-metallic character, which has been suggested for spin filter device applications.[41]

In this work, based on density functional theory (DFT), we systematically investigate the structural, electronic and magnetic properties of the GaSe monolayer doped with vacancy and chemical element. Our main aims are focused on: (1) investigating if vacancy and chemical element doping can induce magnetic moments in non-magnetic 2D GaSe; (2) exploring if 2D GaSe can exhibit n-type character by vacancy or chemical element doping; (3) providing fundamental insights into the spin transport anisotropy of 2D GaSe for its potential application in spin filtering. The presented results will be important for engineering the properties of single-layered GaSe experimentally and may promote efforts towards exploration of 2D materials with novel properties.

2. Computational details

All the spin-polarized DFT calculations are performed using VASP code.[45] The electron structure calculations employing the density functional theory have been rapidly developed during the last decade and it has now become feasible to obtain quite high accuracy for a variety of systems.[46–48] The core electrons and the exchange–correlation energy are described by the projector augmented wave (PAW) potentials[49] and the generalized gradient approximation (GGA) with the Perdew–Burk–Ernzerhof (PBE) functional,[50] respectively. A vacuum region of 15 Å is used to ensure decoupling between neighboring slabs. A plane-wave basis set with a cutoff energy of 500 eV is employed in all the calculations. The vacancies considered in this study include Ga mono-vacancy (V-Ga), Se mono-vacancy (V-Se), Ga di-vacancy ($V\text{-}Ga_2$), Se di-vacancy ($V\text{-}Se_2$), vacancy complexes consisting of one Ga and its nearby three Se atoms ($V\text{-}GaSe_3$), as well as consisting of one Ga–Ga pair and its nearby six Se atoms ($V\text{-}Ga_2Se_6$). For chemical element doping, A group atoms (*e.g.*, Mg, Al, Si) and TM atoms (*e.g.* Sc, Ti, V, Cr, Mn, Fe, Co, Ni, Cu and Zn) are considered to substitute for a single Ga atom, and non-metal atoms (*e.g.* B, C, N, P, O, S, F, Cl, and Br) are considered to substitute for a single Se atom. A 4×4 supercell with a $6 \times 6 \times 1$ Monkhorst–Pack[51] *k*-point mesh is used to model mono- and di-vacancy (V-Ga, V-Se, $V\text{-}Ga_2$ and $V\text{-}Se_2$) decoration and chemical element doping. For $V\text{-}GaSe_3$ and $V\text{-}Ga_2Se_6$ doping, a 7×7 supercell with a $4 \times 4 \times 1$ Monkhorst–Pack *k*-point mesh is employed. All the atom positions are allowed to relax until the Hellmann–Feynman forces are less than 0.02 eV $Å^{-1}$. In order to obtain the magnetic moments, the structure is first completely relaxed by spin-polarized calculations. Bader charge analysis[35] is then performed to investigate the magnetic moment on specific atoms. The accuracy of our calculations is carefully checked based on the GaSe monolayer. In this study, the β phase of GaSe is taken into account. The equilibrium lattice constant of 3.75 Å, the ⟨Ga–Ga⟩ interlayer distance of 2.43 Å along the direction perpendicular to the GaSe plane, the ⟨Ga–Se⟩ bond length of 2.47 Å, and the indirect band gap of 2.23 eV are all in good agreement with other calculations and experimental results[15,52] (see Table 1).

The formation energy of the vacancy-doped system is given by[32]

$$E_f = E_{V\text{-}i@GaSe} - E_{GaSe} + n \times E_{Ga} + m \times E_{Se} \quad (1)$$

where $E_{V\text{-}i@GaSe}$ is the total energy of the supercell containing vacancy defect, and E_{GaSe} is the total energy of the pristine GaSe supercell. E_{Ga} and E_{Se} are the total energies of the isolated Ga and Se atoms, respectively, and n and m are the number of Ga and Se atoms removed from the GaSe monolayer, respectively. For chemical element doping, the binding energy E_b is given by[41]

$$E_b = E_{V\text{-}Ga(Se)@GaSe} + E_X - E_{X@GaSe} \quad (2)$$

Table 1 Calculated lattice constant a, Ga–Ga bond length d⟨Ga–Ga⟩, Ga–Se bond length d⟨Ga–Se⟩, and band gap for the optimized GaSe monolayer. For comparison, other calculation results and the experimental data are listed in parentheses. All lengths and energies are in Å and eV, respectively

	a	d⟨Ga–Ga⟩	d⟨Ga–Se⟩	Band gap
GaSe monolayer	3.75 (3.74)[17,52]	2.43 (2.43)[17] (2.32)[52]	2.47 (2.47)[17] (2.48)[52]	2.23 (2.24)[17]

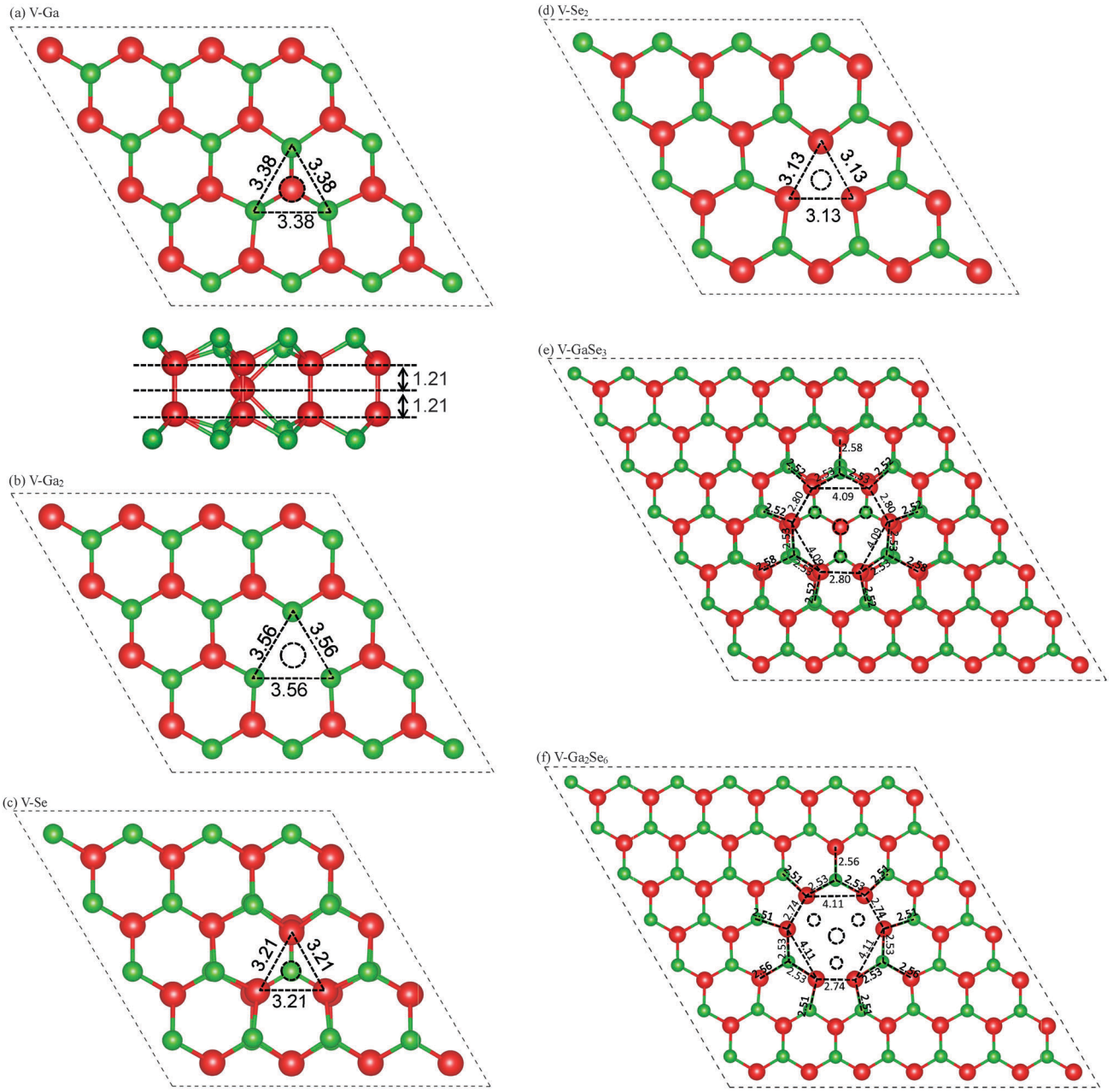

Fig. 1 Schematic view of the geometrical structure for the GaSe monolayer with (a) V-Ga, (b) V-Ga_2, (c) V-Se, (d) V-Se_2, (e) V-$GaSe_3$, and (f) V-Ga_2Se_6. The ⟨Se–Ga⟩ distance, ⟨Se–Se⟩ distance, or ⟨Ga–Ga⟩ distance around the vacancies in the GaSe plane are indicated. For V-Ga, the vertical displacement of the Ga around the vacancy is also indicated. All the distances are in angstroms. Ga and Se atoms are represented by red and green spheres, respectively, and vacancies are marked by the dashed circles.

where $E_{\text{V-Ga(Se)@GaSe}}$ is the energy of the relaxed GaSe structure with Ga (Se) mono-vacancy, E_X is the energy of the isolated X dopant, and $E_{X@GaSe}$ is the energy of the relaxed GaSe doped with X.

3. Results and discussions

3.1 Effects of vacancy on the structural, electronic and magnetic properties of 2D GaSe

3.1.1 Stability and structural properties of vacancy-doped 2D GaSe. Based on eqn (1), the formation energies for V-Ga and V-Ga_2 defects are calculated to be 5.94 and 12.45 eV, respectively. The values for V-Se and V-Se_2 are relatively low, *i.e.*, 5.58 and 11.14 eV, respectively, indicating that anion vacancies are more easily formed in the GaSe monolayer. Comparing with the formation energies of 8.33 eV for single N vacancy and 9.99 eV for single B vacancy in a 5 × 5 × 1 graphitic BN sheet,[32] we find that mono-vacancy can be introduced more easily in GaSe. The formation of V-$GaSe_3$ and V-Ga_2Se_6 in 2D GaSe is considerably energy consuming, as indicated by the large formation energies of 20.02 and 37.56 eV, respectively.

Numerous experimental and theoretical studies have revealed that atomic defects in low-dimension materials often induce structural deformation around the defects.[21–24,27,31,32,43,53,54] For example, strong structural deformation occurs in graphene with one C vacancy.[31] Our calculations show that relaxing the structure of the GaSe monolayer doped with V-Ga causes a dramatic reconstruction, where structural deformations are induced both in the GaSe plane and along the direction normal to the plane. The Ga atom below the vacancy, which is originally in the third Ga sub-layer of perfect GaSe monolayer, moves toward the second Ga sub-layer, with a vertical displacement of 1.21 Å (see Fig. 1(a)). Such behavior is quite different from that in bulk GaSe, in which relaxation of the atomic positions leads to very slight structural deformation.[55] This distinction may have originated from the missing of van der Waals (vdW) interlayer interaction in the GaSe monolayer, as compared with the bulk state. As a vacancy is introduced, the coordination number of the Ga atom changes from 4 (one Ga and three Se atoms) to 6 (six Se atoms). The three Se atoms around the vacancy move closer to each other, forming a regular triangle-like structure. The optimized ⟨Se–Se⟩ distance is 3.38 Å, which is 0.37 Å smaller than that of the pristine GaSe monolayer. If one Ga–Ga dimer is removed from the single-layered GaSe, *i.e.*, a V-Ga_2 defect is created, structural deformation only occurs in the GaSe plane. As presented in Fig. 1(b), the three Se atoms around the vacancy move closer to each other, while the ⟨Se–Se⟩ distance of 3.56 Å is larger than that for V-Ga doping. Our finding that introduction of Ga vacancy causes structural shrink is found to be different from the case of 2D MoS_2 doped with Mo mono-vacancy, in which relaxation of the atomic positions leads to the nearest S atoms moving away from the vacancy.[22]

We now turn to the Se vacancies in the GaSe monolayer. For V-Se doping in the GaSe monolayer, Fig. 1(c) shows that the three Ga atoms around the vacancy move closer to each other, with three equivalent optimized ⟨Ga–Ga⟩ distance of 3.21 Å in the plane, which is 0.54 Å smaller than the intralayer ⟨Ga–Ga⟩ distance of the pristine GaSe monolayer. Different from the case of V-Ga doping, nearly no structure reconstruction occurs along the direction normal to the surface. When two Se atoms are removed from the first and fourth sub-layers of GaSe, *i.e.*, a V-Se_2 defect is created (see Fig. 1(d)), the three Ga atoms in each sub-layer near the vacancy move towards each other, resulting in a ⟨Ga–Ga⟩ distance of 3.13 Å, which is 0.62 Å smaller than the intralayer ⟨Ga–Ga⟩ distance of the pristine GaSe monolayer. Compared with the Se mono-vacancy, creation of Se di-vacancy results in a relatively large structural shrink around the defect. These results differ from those for Ga vacancies, in which Ga di-vacancy induces a smaller structural shrink than Ga mono-vacancy.

In this study, vacancy complexes consisting of one Ga and its nearby three Se atoms (V-$GaSe_3$), as well as one Ga pair and its nearby six Se atoms (V-Ga_2Se_6), are also considered. Similar vacancy complexes, such as V-MoS_3 and V-MoS_6, have been observed in the CVD-grown MoS_2 monolayer.[56] As shown in Fig. 1(e) and (f), both defects induce significant structural deformation. In the meantime, for V-$GaSe_3$ and V-Ga_2Se_6, it is found that only the neighboring Ga atoms around the corners of the vacancy clusters tend to bind with each other, with the ⟨Ga–Ga⟩ distance being 0.95 and 1.01 Å shorter than that of the pristine GaSe monolayer, respectively.

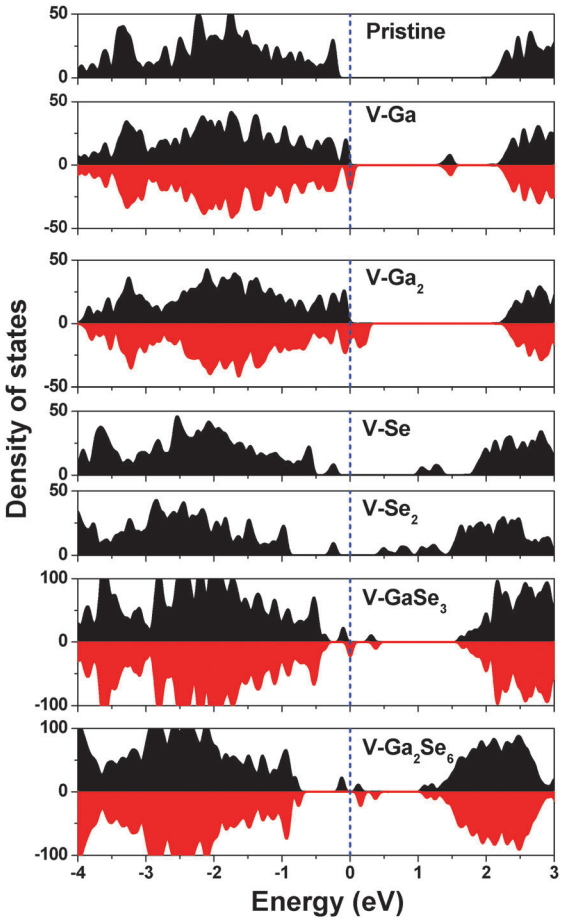

Fig. 2 The spin-resolved total density of states (DOS) for the GaSe monolayer with and without vacancies. The spin up and spin down parts are shaded by black and red colors, respectively. The Fermi levels, which are marked by blue vertical dashed lines, are set to zero.

3.1.2 The electronic and magnetic properties of vacancy-doped 2D GaSe. In the literature it has been reported that the influences of vacancy on the magnetic properties of materials are complex.[20,21,26,27,31,57] For example, in 2D materials doped with anion vacancies, the systems are always non-magnetic. In the case of single-layered TX_2 (T = Mo, W, or Re; X = S, Se, or Te) doped with cation vacancies, only Mo vacancy in $MoSe_2$ can induce magnetism.[26] In MoS_2 the ground state with the MoS_6 vacancy complex is spin-polarized, whereas no magnetic moment can be induced by the MoS_3 vacancy complex.[21] Our calculations show that no magnetic moment is induced by V-Se and V-Se_2 defects in the GaSe monolayer, similar to the case of anion vacancy-doped 2D transition metal dichalcogenides (TMDs).[21] As shown in Fig. 2, the defect levels caused by V-Se and V-Se_2 doping appear near the valence band maximum (VBM) and are located in the band gap of the pristine GaSe, leading to band gap narrowing of 1.00 and 1.57 eV, respectively.

It is interesting to find that introduction of V-Ga and V-Ga_2 has very different effects on the magnetic properties of the GaSe monolayer. For V-Ga, the system energies with and without spin-polarization are comparable to each other and the spin-polarized state has a magnetic moment of 1 μ_B. In the case of V-Ga_2 doping, the spin-polarized state is 0.1 eV more favorable than the un-polarized state, with a magnetic moment of 4 μ_B. Such energy difference will result in high stability of the spin-polarized state under thermal fluctuations,[20] indicating that a dramatic magnetism that may survive at fairly high temperatures can be achieved by creating a Ga di-vacancy in the single-layered GaSe. The spin density distributions for the GaSe monolayer doped with Ga vacancies are illustrated in Fig. 3(a) and (b). For V-Ga, the spin polarized charges are mainly distributed on the three first-neighboring Se atoms and the six next-neighboring Ga–Ga dimers. Compared with Ga mono-vacancy doping, spin density distribution for V-Ga_2 is more delocalized, in which most of the spin polarizations are located on the nearest Se atoms and the rest are distributed on the three second-neighboring Ga–Ga dimers and the twelve third-neighboring Se atoms. The electronic and magnetic properties of the system doped with V-Ga and V-Ga_2 are then further explored by examining the spin-resolved total density of states (DOS) (presented in Fig. 2). It is shown that in both cases the Fermi levels are spinning at the down-spin states and the systems exhibit evidently half-metallic character. The spin-polarization near the Fermi level with intrinsic spin transport anisotropy may enable the cation vacancy-doped systems to be intrinsic spin filtering.[41]

For the GaSe monolayer decorated with V-$GaSe_3$ and V-Ga_2Se_6, our calculations show that both systems are spin-polarized, with magnetic moments of 1 and 2 μ_B, respectively. The spin density distributions for the GaSe monolayer doped with vacancy clusters are quite interesting. As shown in Fig. 3(c) and (d), due to the reduced distances between the cornered Ga atoms near the vacancies, magnetisms are mainly located on the six Ga atoms in the GaSe plane and the three nearest Ga–Ga dimers. Specially, for V-$GaSe_3$, it is interesting to find that anti-ferromagnetic (AFM) couplings[42] are induced between the spins from the Ga atom below the vacancy and those from the defective sub-layer. The magnetic properties can also be clearly observed by the up and down spin channels in the total DOS shown in Fig. 2. Upon vacancy complex creation, four polarized gap states appear in the band gap of 2D GaSe, leading to a dramatic gap decrease for V-Ga_2Se_6 and half-metallic character for V-$GaSe_3$.

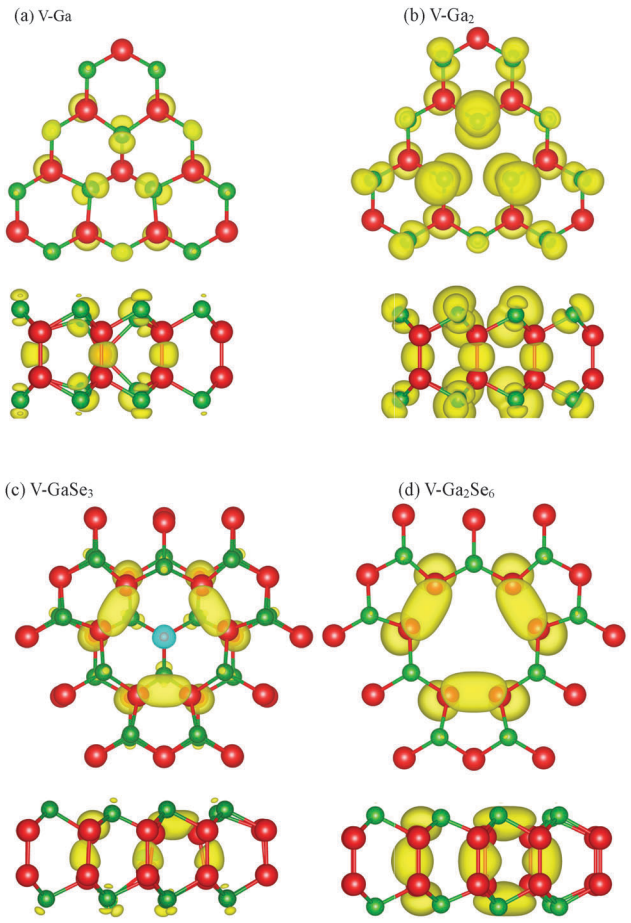

Fig. 3 Top (up) and side (down) views of the isosurface plot of the spin density for the GaSe monolayer with (a) V-Ga, (b) V-Ga_2, (c) V-$GaSe_3$, and (d) V-Ga_2Se_6. Ga and Se atoms are represented by red and green spheres, respectively. The yellow and blue isosurfaces show the positive and negative spin density, respectively.

3.2 Substitution of TM and A group atoms for the Ga-site in the GaSe monolayer

3.2.1 Stability and structural properties of 2D GaSe doped with chemical elements. In this study, substitution of TM

Table 2 Calculated structural and magnetic properties of the GaSe monolayer doped with TM and A group atoms. $d\langle$Se–Se$\rangle$ is the nearest distance between Se atoms around the doping site; $d\langle$Se–X$\rangle$ is the distance between the X dopant and its first-neighboring Se atoms; $d\langle$Ga–X$\rangle$ is the distance between the dopant and its nearest Ga atom; Δd is the vertical distance of the dopant relative to the Ga sub-layer where Ga is replaced; E_b and μ_X are the binding energy and total magnetic moment of the doped system, respectively. The structural parameters for the pristine GaSe monolayer are listed for comparison. All lengths, energies, and magnetic moments are in Å, eV, and μ_B, respectively

Atom	$d\langle$Se–Se$\rangle$	$d\langle$Se–X$\rangle$	$d\langle$Ga–X$\rangle$	Δd	E_b	μ_X
Pristine						
Ga	3.75	2.47	2.43	—	—	0
3d-TM						
Sc	4.07	2.54	2.75	0.41	7.99	0
Ti	3.94	2.45	2.64	0.40	7.77	1
V	3.85	2.40	2.56	0.35	7.06	2
Cr	3.87	2.39	2.51	0.34	5.22	3
Mn	3.90	2.40	2.51	0.30	5.69	4
Fe	3.79	2.38	2.49	0.24	6.05	5
Co	3.74	2.30	2.37	0.23	6.75	2
Ni	3.77	2.29	2.34	0.28	6.11	1
Cu	3.83	2.33	2.40	0.25	4.97	0
Zn	3.83	2.43	2.50	0.14	3.30	1
A group						
Mg	3.98	2.51	2.81	0.24	4.10	1
Al	3.76	2.43	2.48	0.13	6.95	0
Si	3.67	2.36	2.44	0.08	5.69	0

atoms (Sc, Ti, V, Cr, Mn, Fe, Co, Ni, Cu, and Zn) and A group atoms (Mg, Al, Si) is also taken into account. The binding energies (E_b) for the doping systems are firstly calculated and the results are summarized in Table 2. It is found that the binding energies do not change linearly with the TM atomic number. The E_b firstly decrease from Sc to Cr, then increase from Cr to Co, and finally decrease from Co to Zn. Such irregular trends have also been observed in TM-doped graphene.[44] Since the GaSe monolayer is Se-Ga–Ga–Se tetra-layered, the chemical environment of the dopant is complicated, in which the doping atom is bonded to several Se and Ga atoms with both covalent and ionic character. The results indicate that the atomic size and electronic configuration of the dopant, and its interaction with neighbors may all influence the binding energies. It is found that Sc substitution has the largest E_b of 7.99 eV, since the Sc atom has the equivalent valence electrons with the host Ga atom. The smallest E_b of 3.30 eV is found for Zn substitution. These results indicate that strong interaction exists between the TM

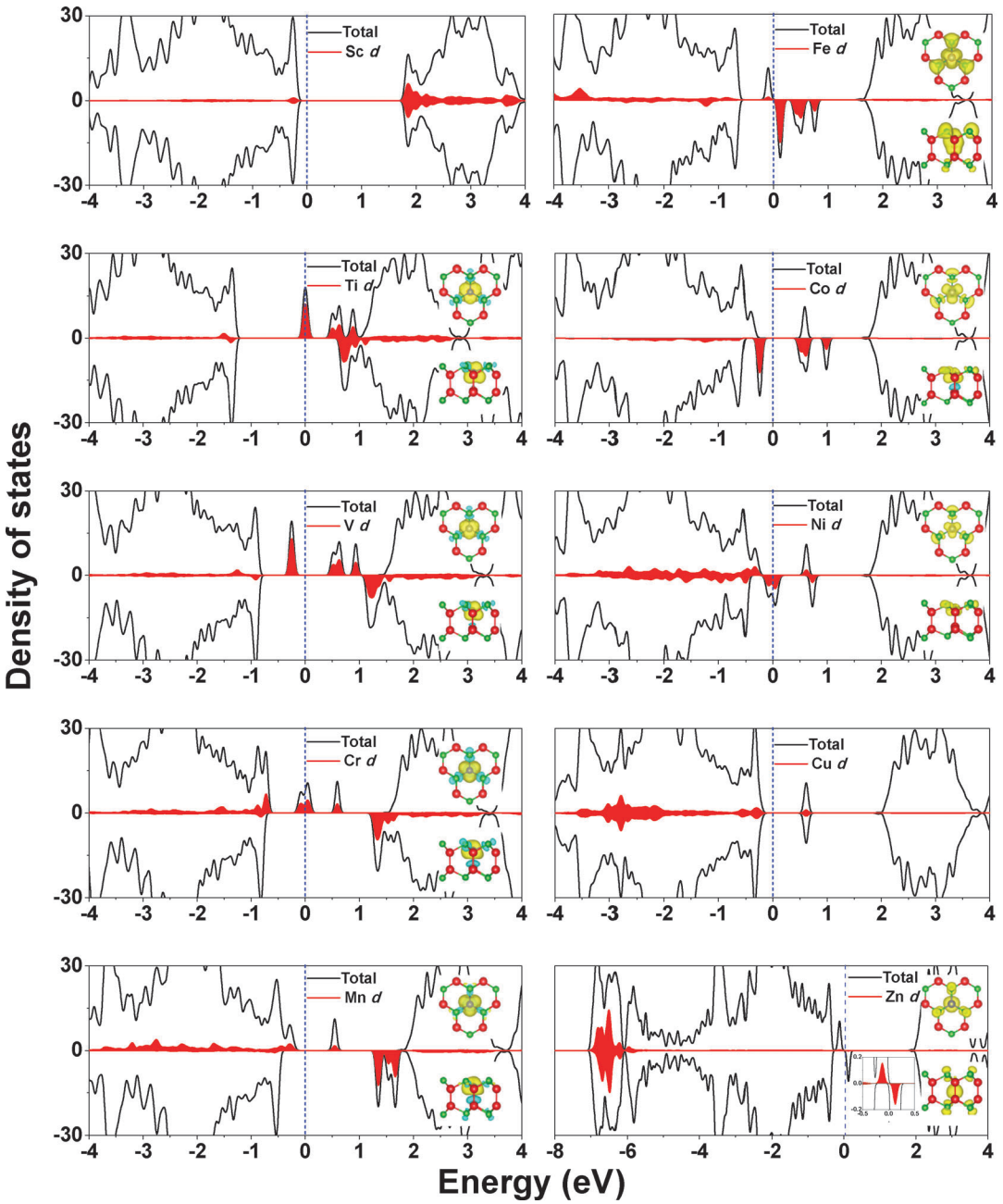

Fig. 4 The spin-resolved total DOS and corresponding partial DOS for the transitional metal-doped GaSe monolayer. The Fermi levels are marked by blue vertical dashed lines and set to zero. The spin density distributions are shown in the insets (the color coding is the same as in Fig. 3). For Zn doping, the inset also shows the zoom-in of the DOS and PDOS close to the Fermi level.

dopants and the GaSe monolayer. The optimized structural properties are also presented in Table 2. As the TM atoms are doped at the Ga site, the $d\langle$Se–Se$\rangle$ values are generally larger than that of the pristine GaSe monolayer (3.75 Å). For Fe, Co and Ni doping, the $d\langle$Se–Se$\rangle$ of 3.74–3.79 Å is comparable to that of the pristine structure. As the atomic number increases, the $d\langle$Se–TM$\rangle$ and $d\langle$Ga–TM$\rangle$ roughly decrease from Sc to Ni, and then increase from Ni to Zn. The largest values are found for the Sc dopant (2.54 and 2.75 Å, respectively), and the smallest ones are for the Ni dopant (2.29 and 2.34 Å, respectively). The vertical deviation of the dopant relative to the Ga sub-layer where Ga is replaced (Δd) is also calculated. It can be seen that the corresponding values vary from 0.14 to 0.41 Å, indicating that structural reconstruction caused by the TM dopant is significant. Among the TM dopants, Zn and Sc exhibit the smallest and largest Δd, respectively. For A group atom (Mg, Al, and Si) doping, the structural parameters of the $d\langle$Se–Se$\rangle$, $d\langle$Se–X$\rangle$, $d\langle$Ga–X$\rangle$, and Δd decrease with increasing atomic number. The largest binding energy of 6.95 eV is found for the Al dopant, since it has equivalent valance electrons and the slightest lattice mismatch with Ga.

3.2.2 Effects of TM and A group atom doping on the electronic and magnetic properties of 2D GaSe. The effects of chemical element doping on the electronic properties of GaSe monolayer are investigated by the spin-resolved total DOS, orbital-projected partial DOS (PDOS). As shown in Fig. 4 and 5, except the substitutions of Sc and Al, which are isoelectronic to Ga, other dopants can induce impurity levels located in the band gap of the pristine 2D GaSe. The Mg dopant with less valance electrons than Ga is expected to exhibit p-type doping character. As shown in Fig. 5, the spin-up defect level of Mg is situated closely to the VBM. The corresponding down-spin level departs from the VBM, resulting in a spin splitting of $\sim$0.5 eV, which may enhance the carrier activation energies.[39] A previous study on the Mg-doped GaSe nanosheets has suggested that effective p-doping can be achieved by increasing the dopant concentration to 5.6%, with both spin-up and spin-down defect levels moving closer to the VBM.[17] The dopants with more valance electrons than Ga are expected to act as sources of n-type doping for GaSe. Among all the dopants, the Si atom is found to be the best candidate for n-type doping of GaSe, since the binding energy E_b is as high as 5.69 eV and the associated defect level is situated in the conduction band of GaSe, as shown in Fig. 5. Besides, our calculations show that upon Ti, Cr, and Ni doping, the systems exhibit intrinsic spin transport anisotropy, *i.e.*, half-metallicity. For the Ti and Cr substitution, the Fermi levels are spinning at the up-spin gap states, and band gaps of 1.64 and 2.05 eV are found in the down-spin parts, respectively. In the case of Ni doping, the Fermi level crosses the down-spin gap states, and a gap of 0.86 eV is found for the up-spin part. With spin-polarized electrons located around the Fermi level, these doped systems exhibit potential for application in spin filter devicess.[41]

While the ground state of the GaSe monolayer is non-spin-polarized, doping TM atoms can greatly modify the magnetic properties of the nanomaterial. Except for Sc and Cu, the remaining eight TM dopants can induce several magnetic moments in 2D GaSe (see Table 2). As the number of electrons in the partially filled d shell grows, the magnetic moments firstly increase linearly from Ti to Fe, reaching a maximum of 5 μ_B, and then decrease from Co to Ni. It seems that the magnetic moments induced by TM atoms follow a simple trend of the number of extra d electrons of the TM atoms, whereas our analysis shows that the magnetism originating from the Ga and (or) Se atoms nearby the dopants is not negligible, as revealed by the spin density distribution shown in the insets of Fig. 4. Taking an example of Co, the magnetic moment of 2 μ_B is contributed by the dopant (1.66 μ_B), the first neighboring Se atoms (0.30 μ_B) and the Ga atom below the dopant ($-$0.05 μ_B). Of the full d-shell substitutions, Cu doping results in a non-magnetic ground state, whereas Zn can induce a magnetic moment of 1 μ_B. About half of the magnetism in Zn-doped GaSe comes from the neighboring Se (0.56 μ_B), and the others are originated from Zn (0.12 μ_B) and its nearby Ga (0.19 μ_B) atoms. These results are quite different from those obtained for Cu and Zn-doped MoS_2, where no magnetic moments are

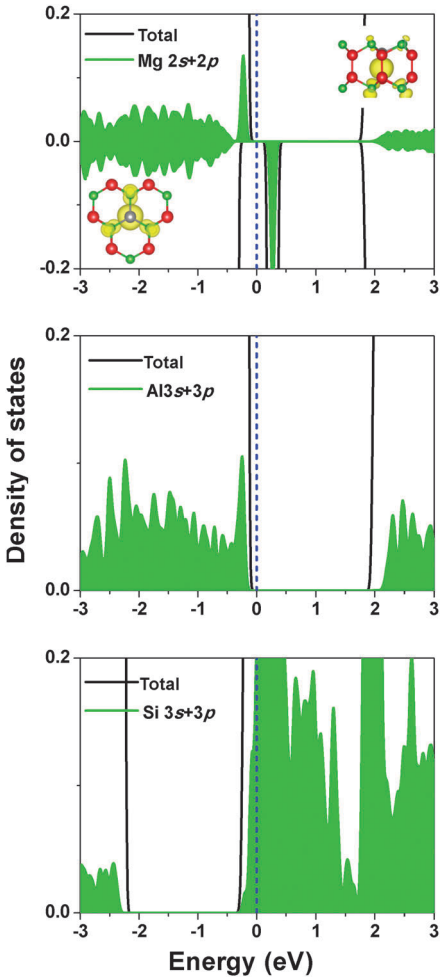

Fig. 5 The spin-resolved total DOS and PDOS for the GaSe monolayer doped with A group atoms. The spin density distributions are shown in the insets (the color coding is the same as in Fig. 3). The Fermi levels are marked by blue vertical dashed lines and set to zero.

carried for Zn doping, whereas Cu can induce unexpected large magnetism originating from the hybridization between Cu 3d states and S 3p states.[40] For dopants without d electrons, *i.e.*, A group element doping, only Mg can induce magnetic moment (1 μ_B), which is in good agreement with the previous study.[17] As Al is isoelectronic to the Ga atom, the replacement of Ga by Al does not induce any magnetism. For Si doping, Bader charge analysis shows that one electron of Si is transferred to the GaSe monolayer, which results in Si being isoelectronic to Ga and the non-magnetic ground state.

To investigate the effects of d electrons on the electronic and magnetic properties of 2D GaSe, Ni, Zn and Mg are selected to represent partially filled d-shells doping, full d-shells and no d valance electrons doping, respectively. For Ni doping (see Fig. 6), there is a strong hybridization between Ni 3d states and Se 4p states in a wide range of energy. As Ni has the shortest $d\langle$Se–TM$\rangle$ of 2.29 Å among the ten TM dopants and the binding energy is as high as 6.11 eV, it is expected that the Ni atom can be bound to the surrounding Se atoms strongly with relatively more covalent bonding. However, unlike the situation of Nb atoms in the NbS_2 structure,[58] the covalent bonding interaction does not quench the magnetism of the Ni atom, leading to the splitting of spin-up and spin-down states. The Mn-doped MoS_2 nanosheet also undergoes spin splitting, in which the magnetism is mainly originated from Mn 3d states.[41] This is somewhat different from our case, since the magnetic moment is mainly caused by the strong hybridization between the 4p states of the neighboring Se atom (0.32 μ_B) and the Ni 3d spin states (0.61 μ_B). Our calculation results indicate that similar DOS, PDOS and spin density distributions (see the insets in Fig. 4 and 5) can be found for Zn and Mg doping cases. Taking the example of Mg doping, as shown in the inset of Fig. 5, the main parts of the polarized charges are not distributed on the Mg dopant, but located on the Se and Ga atoms nearby the dopant. These results can be confirmed by the total and partial DOS shown in Fig. 7, in which the magnetization mainly originates from the 4p states of the neighboring Se atoms (0.51 μ_B), with hybridization of the 4s, 4p

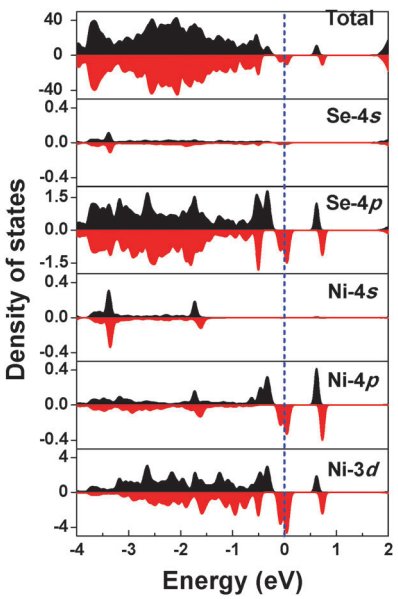

Fig. 6 The spin-resolved total DOS and orbital-projected PDOS for the Ni-substituted GaSe monolayer. The spin up and spin down parts are shaded by black and red colors, respectively. The Fermi levels are marked by blue vertical dashed lines and set to zero.

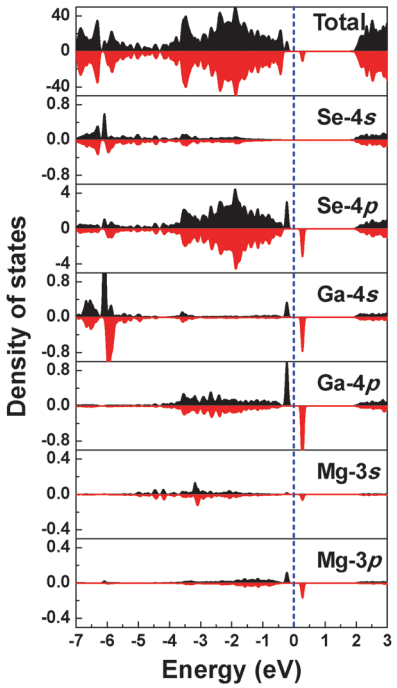

Fig. 7 The spin-resolved total DOS, and corresponding PDOS for the Mg-substituted GaSe monolayer. The spin up and spin down parts are shaded by black and red colors, respectively. The Fermi levels are marked by blue vertical dashed lines and set to zero.

Table 3 Calculated structural and magnetic properties of the GaSe monolayer doped with A group atoms. $d\langle$Ga–Ga$\rangle$ is the nearest distance between the first-neighboring Ga atoms around the doping site; $d\langle$Ga–X$\rangle$ is the distance between the dopant and its first-neighboring Ga atom; $d\langle$Se–X$\rangle$ is the distance between the dopant and the nearest Se atom; Δd is the vertical distance of the dopant relative to the Se sub-layer where Se is replaced; E_b is the binding energy of the doped system; μ_X is the total magnetic moment of the doped system. The structural parameters for the pristine GaSe monolayer are listed for comparison. All lengths, energies, and magnetic moments are in Å, eV, and μ_B, respectively

Atom	$d\langle$Ga–Ga$\rangle$	$d\langle$Ga–X$\rangle$	$d\langle$Se–X$\rangle$	Δd	E_b	μ_X
Pristine						
Se	3.75	2.47	4.82	—	—	0
A group						
B	3.56	2.07	4.02	−0.85	4.97	1
C	3.39	1.99	4.10	−0.76	6.42	0
N	3.32	1.97	4.15	−0.73	5.72	1
O	3.35	2.00	4.24	−0.73	7.50	0
F	3.63	2.18	4.23	−0.68	4.90	0
P	3.72	2.33	4.51	−0.25	4.59	1
S	3.67	2.37	4.71	−0.15	6.15	0
Cl	4.10	2.55	4.46	−0.35	3.19	0
Br	4.23	2.67	4.56	−0.24	2.70	0

states of the nearest Ga atom (0.38 μ_B) and the 4s, 4p states of Mg atom (0.05 μ_B).

3.3 Substitution of A group atoms for the Se-site in the GaSe monolayer

3.3.1 Stability and structural properties of 2D GaSe doped with chemical elements. In this study, B, C, N, O, F, P, S, Cl, and Br atoms are considered to substitute for the Se-site in the GaSe monolayer. The binding energies are firstly calculated, which are based on eqn (2), and the results are summarized in Table 3. The O substituent, which is isoelectronic to the Se atom, has the largest binding energy of 7.50 eV. The lowest binding energy of 2.70 eV is found for Br substitution. These results indicate that similar to the Ga substitution, all the considered dopants can strongly interact with the GaSe monolayer. The structural properties of the doping systems are presented in Table 3. For dopants of B, C, N, O, F, P and S, and F, the $d\langle$Ga–Ga$\rangle$, $d\langle$Ga–X$\rangle$ and $d\langle$Se–X$\rangle$ are all smaller than the corresponding bond distance in the pristine GaSe monolayer, indicative of the local structure shrink around the doping site. As for Cl and Br, the neighboring Ga atoms

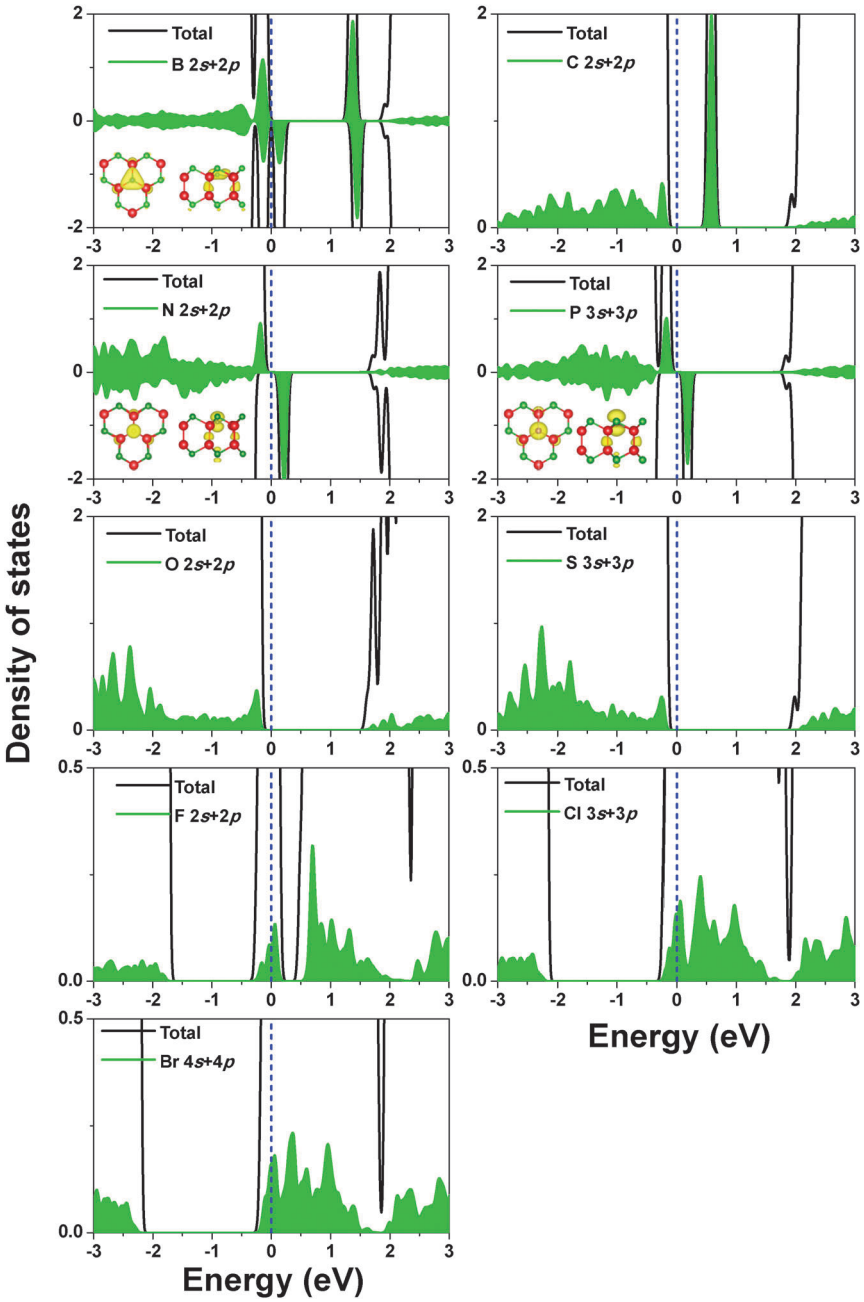

Fig. 8 The spin-resolved total DOS and corresponding PDOS for the GaSe monolayer doped with A group atoms. The Fermi levels are marked by blue vertical dashed lines and set to zero. The spin density distributions are shown in the insets (the color coding is the same as in Fig. 3).

tend to move away from each other, while the Se atoms move toward the dopant. Contrary to the situation of Ga substitution, where the TM and A group dopant moves toward the first sub-layer, doping A group atoms at the Se site usually results in the dopant moving away from the first sub-layer, leading to negative values of all the Δd. Among the nine dopants, C has the largest vertical displacement of 0.76 Å, while the isoelectronic S has a tiny Δd of 0.15 Å.

3.3.2 Effects of A group atom doping on the electronic and magnetic properties of 2D GaSe. The spin-resolved total and partial DOS, along with the spin density distribution, for 2D GaSe doped with A group atoms are illustrated in Fig. 8. Here, based on the number of valance electrons, we classify the doping atoms into three groups: (1) atoms of B, C, N, and P with less p electrons than the Se atom; (2) halogen atoms (F, Cl and Br) with more p electrons than the Se atom; (3) atoms of O and S that are isoelectronic to the Se atom.

Atoms of B, C, N, and P exhibit potential as the source for p-type doping for the GaSe monolayer. The ground state of B-doped GaSe is magnetic. The calculated magnetic moment is 1 μ_B per B atom, which is mainly contributed by B atoms (0.21 μ_B), nearby Ga atoms (0.34 μ_B) and second-neighboring Se atoms (0.36 μ_B). Upon B doping at the Se site, several polarized defect levels appear in the GaSe band gap, among which one spin-up channel and two spin-down channels are near the VBM. However, these defect levels are not shallow enough to provide an ideal p-type doping for the GaSe monolayer, since the activation energy is expected to be relatively high.[39] Similar total and partial DOS distributions are found for N and P doping. Both N and P dopants can also induce a magnetic moment of 1 μ_B, and about half of the magnetism (0.45 μ_B) originates from the doping elements. With one p valance electron less than the Se atom, both N and P cause spin splitting near the VBM of GaSe, with the up-spin state being occupied and the down-spin state empty. The large spin splitting ($\sim$0.5 eV) for N and P doping may make them unsuitable for efficient p-type doping for GaSe. However, effective p-type doping of the GaSe monolayer probably can be achieved by doping high concentrations of considered elements.[17] In the case of the C dopant, it gains an electron from the host monolayer, leading to the nonmagnetic ground state. Similar to the situation of C-doped ReS_2,[39] an unoccupied defect level is induced deeply in the band gap of GaSe.

For F, Cl, and Br-doped GaSe monolayers, the ground states of these systems are all non-spin-polarized. As shown in Fig. 8, by donating the extra electrons to the conduction band of the GaSe, halogen atoms can cause an upward shift of the Fermi level, leading to metallic ground states. As compared with F, the considerably shallow defect levels of Cl and Br indicate that they may act as better sources for n-type doping. Considering that Br has a smaller binding energy than Cl, Cl may be a better candidate.

As atoms of O and S are isoelectronic to the Se atom, they do not induce impurity levels in the GaSe band gap. However, the valance and conduction band edges have been modified dramatically. As compared with S, doping O at the Se-site leads to larger band gap reduction. Çakır *et al.*[39] suggested that congeners doping can be utilized to tune the band gap consecutively by controlling the doping concentration without destroying the main electronic structure of the host materials. This strategy may also be appropriate for manipulating the band gap of the GaSe monolayer.

4. Conclusion

In summary, a systematic DFT study has been carried out on 2D GaSe to investigate how vacancy and chemical element doping influence its electronic and magnetic properties. Based on the DFT calculation, we have demonstrated that the new synthesized 2D GaSe can be functionalized by vacancy and chemical element doping to achieve novel electronic and magnetic properties. Our results show that magnetism can be induced by decorating vacancies of V-Ga, V-Ga_2, V-$GaSe_3$, and V-Ga_2Se_6, with magnetic moments of 1, 4, 1, and 2 μ_B, respectively.

Chemical element doping at the Ga- or Se-site provides another way to modify the magnetisms of the GaSe monolayer. As A group (*e.g.*, Mg, Al, Si) and TM atoms (*e.g.* Sc, Ti, V, Cr, Mn, Fe, Co, Ni, Cu and Zn) substitute for the Ga-site, magnetism is induced in most cases, except for Sc, Cu, Al and Si. However, the microscopic mechanisms for magnetism induction are different. For dopants with a partially filled d-shell, such as Ni doping, the induced magnetic moment is mainly originated from the unsaturated d electrons of the dopant and the 4p states of the nearby Se atoms; for dopants with a full d-shell and without d electrons, such as Zn and Mg doping, the magnetic moments mainly stem from the 4p states of the neighboring Se atoms and the 4s, 4p states of the nearest Ga atom. As an alternative, substitution of the A group atoms at the Se-site can also induce magnetism. It is found that the ground states of B, N, and P-doped GaSe have magnetic moments of 1 μ_B.

Meanwhile, the GaSe monolayer doped with V-Ga_2, V-$GaSe_3$, Ti, Cr, and Ni exhibit half-metallic features, which are promising for low-dimensional spintronic device application. Our calculations also show that it is possible to obtain an n-type GaSe monolayer by substitution of Si for Ga or substitution of Cl for Se. These results suggest that the newly synthesized 2D GaSe can be functionalized by vacancy and chemical element doping to achieve novel electronic and magnetic properties.

Acknowledgements

This work was supported by the NSAF Joint Foundation of China (Grant No. U1330103), the National Natural Science Foundation of China (Grant No. 51201026), the Fundamental Research Funds for the Central Universities of China (Grant No. ZYGX2011J038), and Prof. Xiao Liu's Scientific Research Starting Funding of Young Qianren Plan (A10002010401005). H. Y. Xiao acknowledges the Scientific Research Starting Funding of

University of Electronic Science and Technology of China (Grant No. Y02002010401085). The theoretical calculations were performed using the supercomputer resources at TianHe-1 located at National Supercomputer Center in Tianjin.

References

1 K. S. Novoselov, V. I. Fal'ko, L. Colombo, P. R. Gellert, M. G. Schwab and K. Kim, *Nature*, 2012, **490**, 192.
2 F. G. Schwierz, *Nat. Nanotechnol.*, 2010, **5**, 487.
3 K. Sengupta and G. Baskaran, *Phys. Rev. B: Condens. Matter Mater. Phys.*, 2008, **77**(4), 045417.
4 M. Hentschel and F. Guinea, *Phys. Rev. B: Condens. Matter Mater. Phys.*, 2007, **76**(11), 115407.
5 A. K. Geim and K. S. Novoselov, *Nat. Mater.*, 2007, **6**, 183.
6 B. Dora and P. Thalmeier, *Phys. Rev. B: Condens. Matter Mater. Phys.*, 2007, **76**(11), 115435.
7 Y. B. Zhang, Y. W. Tan, H. L. Stormer and P. Kim, *Nature*, 2005, **438**, 201.
8 V. P. Gusynin and S. G. Sharapov, *Phys. Rev. Lett.*, 2005, **95**, 146801.
9 K. S. Novoselov, A. K. Geim, S. V. Morozov, D. Jiang, M. I. Katsnelson, I. V. Grigorieva, S. V. Dubonos and A. A. Firsov, *Nature*, 2005, **438**(7065), 197.
10 K. S. Novoselov, A. K. Geim, S. V. Morozov, D. Jiang, Y. Zhang, S. V. Dubonos, I. V. Grigorieva and A. A. Firsov, *Science*, 2004, **306**, 666.
11 X. F. Li, M. W. Lin, A. A. Puretzky, J. C. Idrobo, C. Ma, M. F. Chi, M. Yoon, C. M. Rouleau, I. I. Kravchenko, D. B. Geohegan and K. Xiao, *Sci. Rep.*, 2014, **4**, 5497.
12 D. J. Late, B. Liu, J. J. Luo, A. M. Yan, H. S. S. R. Matte, M. Grayson, C. N. R. Rao and V. P. Dravid, *Adv. Mater.*, 2012, **24**, 3549.
13 D. J. Late, B. Liu, H. S. S. R. Matte, C. N. R. Rao and V. P. Dravid, *Adv. Funct. Mater.*, 2012, **22**(9), 1894.
14 A. Kuhn, A. Chevy and R. Chevalier, *Phys. Status Solidi A*, 1975, **31**, 469.
15 Y. D. Ma, Y. Dai, M. Guo, L. Yu and B. B. Huang, *Phys. Chem. Chem. Phys.*, 2013, **15**, 7098.
16 Z. Y. Zhu, Y. C. Cheng and U. Schwingenschlo, *Phys. Rev. Lett.*, 2012, **108**, 266805.
17 Y. T. Peng, C. X. Xia, H. Zhang, T. X. Wang, S. Y. Wei and Y. Jia, *Phys. Chem. Chem. Phys.*, 2014, **16**, 18799.
18 H. L. Zhuang and R. G. Hennig, *Chem. Mater.*, 2013, **25**(15), 3232.
19 S. R. Zhang, S. F. Zhu, B. J. Zhao, L. H. Xie and K. H. Song, *Physica B*, 2014, **436**, 188.
20 S. Horzum, D. Çakır, J. Suh, S. Tongay, Y. S. Huang, C. H. Ho, J. Wu, H. Sahin and F. M. Peeters, *Phys. Rev. B: Condens. Matter Mater. Phys.*, 2014, **89**, 155433.
21 H. L. Zheng, B. S. Yang, D. D. Wang, R. L. Han, X. B. Du and Y. Yan, *Appl. Phys. Lett.*, 2014, **104**, 132403.
22 W. Zhou, X. L. Zou, S. Najmaei, Z. Liu, Y. M. Shi, J. Kong, J. Lou, P. M. Ajayan, B. I. Yakobson and J. C. Idrobo, *Nano Lett.*, 2013, **13**(6), 2615.
23 B. Ouyang and J. Song, *Appl. Phys. Lett.*, 2013, **103**, 102401.
24 P. T. Araujoa, M. Terrones and M. S. Dresselhaus, *Mater. Today*, 2012, **15**(3), 98.
25 H. P. Komsa, J. Kotakoski, S. Kurasch, O. Lehtinen, U. Kaiser and A. V. Krasheninnikov, *Phys. Rev. Lett.*, 2012, **109**(3), 035503.
26 Y. D. Ma, Y. Dai, M. Guo, C. W. Niu, J. B. Lua and B. B. Huang, *Phys. Chem. Chem. Phys.*, 2011, **13**, 15546.
27 R. Shidpoura and M. Manteghian, *Nanoscale*, 2010, **2**, 1429.
28 P. O. Lehtinen, A. S. Foster, Y. C. Ma, A. V. Krasheninnikov and R. M. Nieminen, *Phys. Rev. Lett.*, 2004, **93**, 187202.
29 S. Hosaka, S. Hosoki, T. Hasegawa, H. Koyanagi, T. Shintani and M. Miyamoto, *J. Vac. Sci. Technol., B*, 1995, **13**(6), 2813.
30 S. Hosoki, S. Hosaka and T. Hasegawa, *Appl. Surf. Sci.*, 1992, **60**, 643.
31 O. V. Yazyev and L. Helm, *Phys. Rev. B: Condens. Matter Mater. Phys.*, 2007, **75**, 125408.
32 M. S. Si and D. S. Xue, *Phys. Rev. B: Condens. Matter Mater. Phys.*, 2007, **75**, 193409.
33 G. Guisbiers, *J. Phys. Chem. C*, 2011, **115**(6), 2616.
34 N. Shehata, K. Meehan, I. Ashry, I. Kandas and Y. Xu, *Sens. Actuators, B*, 2013, **183**, 179.
35 E. Sanville, S. D. Kenny, R. Smith and G. Henkelman, *J. Comput. Chem.*, 2007, **28**, 899.
36 K. Dolui, I. Rungger, C. D. Pemmaraju and S. Sanvito, *Phys. Rev. B: Condens. Matter Mater. Phys.*, 2013, **88**, 075420.
37 M. R. Laskar, D. N. Nath, L. Ma and E. W. Lee, *Appl. Phys. Lett.*, 2014, **104**, 092104.
38 Y. M. Shi, J. K. Huang, L. M. Jin, Y. T. Hsu, S. F. Yu, L. J. Li and H. Y. Yang, *Sci. Rep.*, 2013, **3**, 1839.
39 D. Çakır, H. Sahin and F. M. Peeters, *Phys. Chem. Chem. Phys.*, 2014, **16**, 16771.
40 W. S. Yun and J. D. Lee, *Phys. Chem. Chem. Phys.*, 2014, **16**, 8990.
41 Y. G. Zhou, Q. L. Su, Z. G. Wang, H. Q. Deng and X. T. Zu, *Phys. Chem. Chem. Phys.*, 2013, **15**, 18464.
42 R. Mishra, W. Zhou, S. J. Pennycook, S. T. Pantelides and J. C. Idrobo, *Phys. Rev. B: Condens. Matter Mater. Phys.*, 2013, **88**, 144409.
43 A. H. Zhang, H. F. Teoh, Z. X. Dai, Y. P. Feng and C. Zhang, *Appl. Phys. Lett.*, 2011, **98**, 023105.
44 A. V. Krasheninnikov, P. O. Lehtinen, A. S. Foster, P. Pyykkö and R. M. Nieminen, *Phys. Rev. Lett.*, 2009, **192**, 126807.
45 G. Kresse and J. Furthmuller, *Phys. Rev. B: Condens. Matter Mater. Phys.*, 1996, **54**(16), 11169.
46 H. Y. Xiao, X. T. Zu, Y. F. Zhang and L. Yang, *J. Chem. Phys.*, 2005, **122**, 174704.
47 H. Y. Xiao and D. Q. Xie, *Surf. Sci.*, 2004, **558**, 15.
48 Z. L. Zhang, H. Y. Xiao, X. T. Zu, F. Gao and W. J. Weber, *J. Mater. Res.*, 2009, **24**(4), 1335.
49 P. E. Blöchl, *Phys. Rev. B: Condens. Matter Mater. Phys.*, 1994, **50**(24), 17953.
50 J. P. Perdew, K. Burke and M. Ernzerhof, *Phys. Rev. Lett.*, 1996, **77**, 3865.

51 H. J. Monkhorst and J. D. Pack, *Phys. Rev. B: Condens. Matter Mater. Phys.*, 1976, **13**(12), 5188.
52 R. W. G. Wyckoff, *Crystal Structures.*, Interscience Publishers, inc., New York, 1948.
53 J. C. Meyer, A. Chuvilin, G. A. Siller, J. Biskupek and U. Kaiser, *Nano Lett.*, 2009, **9**, 2683.
54 C. H. Jin, F. Lin, K. Suenaga and S. Iijima, *Phys. Rev. Lett.*, 2009, **102**, 195505.
55 Z. Rak, S. D. Mahanti, K. C. Mandal and N. C. Fernelius, *J. Phys. Chem. Solids*, 2009, **70**, 344.
56 W. Zhou, X. L. Zou, S. Najmaei, Z. Liu, Y. Shi, J. Kong, J. Lou, P. M. Ajayan, B. I. Yakobson and J. C. Idrobo, *Nano Lett.*, 2013, **13**, 2615.
57 R. F. Liu and C. Cheng, *Phys. Rev. B: Condens. Matter Mater. Phys.*, 2007, **76**, 014405.
58 Y. G. Zhou, Z. G. Wang, P. Yang, X. T. Zu, L. Yang, X. Sun and F. Gao, *ACS Nano*, 2012, **6**(11), 9727.

